





Optimal Thresholds for Fracton Codes and Random Spin Models with Subsystem Symmetry

Hao Song (宋昊)^{1,2,3} Janik Schönmeier-Kromer,^{4,5} Ke Liu (刘科子竞)^{4,5,*} Oscar Viyuela,^{6,7}
Lode Pollet^{4,5,8} and M. A. Martin-Delgado^{3,†}

¹CAS Key Laboratory of Theoretical Physics, Institute of Theoretical Physics, Chinese Academy of Sciences, Beijing 100190, China

²Department of Physics and Astronomy, McMaster University, Hamilton, Ontario L8S 4M1, Canada

³Departamento de Física Teórica, Universidad Complutense, 28040 Madrid, Spain

⁴Arnold Sommerfeld Center for Theoretical Physics, University of Munich, Theresienstr. 37, 80333 München, Germany

⁵Munich Center for Quantum Science and Technology (MCQST), Schellingstr. 4, 80799 München, Germany

⁶Department of Physics, Massachusetts Institute of Technology, Cambridge, Massachusetts 02139, USA

⁷Department of Physics, Harvard University, Cambridge, Massachusetts 02318, USA

⁸Wilczek Quantum Center, School of Physics and Astronomy, Shanghai Jiao Tong University, Shanghai 200240, China



(Received 17 December 2021; accepted 11 October 2022; published 30 November 2022)

Fracton models provide examples of novel gapped quantum phases of matter that host intrinsically immobile excitations and therefore lie beyond the conventional notion of topological order. Here, we calculate optimal error thresholds for quantum error correcting codes based on fracton models. By mapping the error-correction process for bit-flip and phase-flip noises into novel statistical models with Ising variables and random multibody couplings, we obtain models that exhibit an unconventional subsystem symmetry instead of a more usual global symmetry. We perform large-scale parallel tempering Monte Carlo simulations to obtain disorder-temperature phase diagrams, which are then used to predict optimal error thresholds for the corresponding fracton code. Remarkably, we found that the X-cube fracton code displays a minimum error threshold (7.5%) that is much higher than 3D topological codes such as the toric code (3.3%), or the color code (1.9%). This result, together with the predicted absence of glass order at the Nishimori line, shows great potential for fracton phases to be used as quantum memory platforms.

DOI: [10.1103/PhysRevLett.129.230502](https://doi.org/10.1103/PhysRevLett.129.230502)

Introduction.—The study of quantum phases constitutes a cornerstone of quantum many-body physics and can potentially enable technological advances. Among its modern applications is the possible realization of a fully fledged quantum computer by means of fault-tolerant methods for processing quantum information [1–3]. Topological codes [4,5] stand among the best options to performing fault-tolerant quantum computation due to their high thresholds and linear scaling of the system qubit resources [6,7]. Nevertheless, 2D topological stabilizer codes like the most studied surface code [4,6,8] permit only topological implementations of Clifford gates [9], while non-Clifford gates are necessary for realizing the desired quantum advantages [10], motivating the quest for new 3D codes. Fracton models [11–27] represent a generalization to 3D topological orders and provide alternatives to quantum memories beyond the standard paradigm of topological computing. These models host intrinsically

immobile pointlike excitations called fractons [15] which make a key difference from conventional topological orders and have potential beneficial applications. While a few decoders [28,29] and several experimental platforms [30–32] are proposed, the theoretical limit on error thresholds of fracton codes is unexplored, which is nevertheless crucial for devising new decoders and for justifying the practical relevance of fracton codes.

The goal of this Letter is to investigate how a fracton model behaves as an active error correcting code against stochastic Pauli errors, which are widely used for benchmarking quantum memories. We have defined error corrections in the presence of a subextensive ground state degeneracy and computed the optimal thresholds for one of the most representative fracton models in three dimensions—the X-cube model [16]. We address the problem by a combination of theoretical analyses and numerical simulations. Using a statistical-mechanical mapping method [6] that has previously produced error thresholds for codes beyond those for which it was initially conceived [33–40], we derive two statistical models related to Pauli errors of the X-cube model, in the formulation of classical spin variables that are suited for simulations. The numerical simulation of statistical models in three dimensions with randomness is generally

Published by the American Physical Society under the terms of the [Creative Commons Attribution 4.0 International license](https://creativecommons.org/licenses/by/4.0/). Further distribution of this work must maintain attribution to the author(s) and the published article's title, journal citation, and DOI.

challenging, and the required resources are even higher for our models as they possess lower-dimensional subsystem symmetries rather than a more conventional global symmetry. Only by utilizing state-of-the-art parallel tempering Monte Carlo methods and performing large-scale simulations have we been able to compute various many-body correlation functions and determine the phase diagrams for the two statistical models up to moderate error rates.

We estimate the optimal error thresholds of the X-cube code against bit-flip (X) and phase-flip errors (Z) as $p_c^X \simeq 0.152(4)$ and $p_c^Z \simeq 0.075(2)$, respectively. The minimum of these thresholds is remarkably higher than what was found in conventional 3D topological codes such as the toric code (0.033) [41,42] and the color code (0.019) [38], which signals the potential of the X-cube model as a fault-tolerant quantum memory. This is further confirmed by the analytical result that the Nishimori line is free of fracton glass order through which the resilience of the quantum code may be lost (see Supplemental Material [43]). In addition, our results represent the first study of spin models with both subsystem symmetries and quenched random disorder in three dimensions, hence are also of interest for the statistical mechanics community.

X-cube model as quantum memory.—Consider a cubic lattice \mathcal{L} with periodic boundary condition (PBC). We introduce a qubit to every edge ℓ and define stabilizer generators A_c and B_v^μ at each unit cube c and vertex v of the lattice. Specifically, A_c is defined to be the tensor product of Pauli X operators on the 12 edges of a cube, and B_v^μ is a tensor product of Pauli Z operators on the four edges adjacent to a vertex and perpendicular to the spatial direction $\mu = x, y, z$. Namely,

$$A_c := \prod_{\ell \in c} X_\ell, \quad B_v^\mu := \prod_{\ell \in v: \ell \perp \mu} Z_\ell, \quad (1)$$

as visualized in Fig. 1. For convenience, we label the set of qubits as \mathcal{Q} and those of stabilizer generators as $\mathcal{A} := \{A_c\}$ and $\mathcal{B} := \{B_v^x, B_v^y\}$, respectively.

The X-cube model is a paradigmatic fracton model constructed by summing over these stabilizer generators,

$$H_{\text{X-cube}} = -\sum_{c \in \mathcal{L}} A_c - \sum_{v \in \mathcal{L}} (B_v^x + B_v^y + B_v^z). \quad (2)$$

As A_c and B_v^μ commute, this Hamiltonian is exactly solvable [16], and its ground states satisfy $A_c = 1$ and $B_v^\mu = 1$ for all c, v, μ . The elementary excitations are two types of gapped topological defects. A unit cube with $A_c = -1$ is referred to as a *fracton* (solid cyan cube in Fig. 1), which is an intrinsically *immobile* defect. A vertex with $B_v^\mu = 1$ but $B_v^{\nu \neq \mu} = -1$ corresponds to an excitation termed a *lineon* (red ellipsoid in Fig. 1), which can move along the μ direction but is immobile in the two directions $\nu \neq \mu$. The three possible lineons at each vertex are subject to a constraint $B_v^x B_v^y B_v^z = 1$.

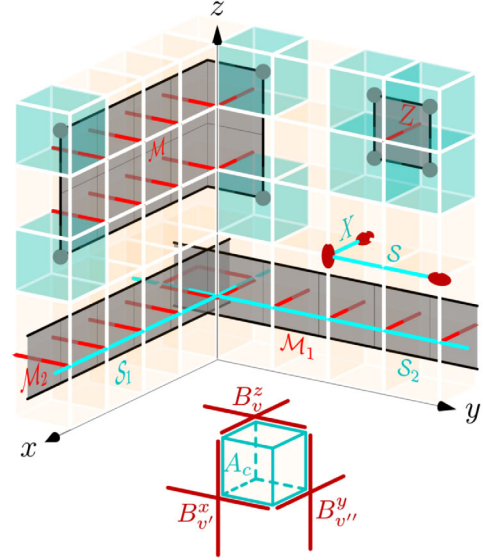


FIG. 1. Stabilizer generators, excitations, and logical operators of the X-cube model. A physical qubit is assigned to each edge (ℓ) of the lattice. A Pauli X (Z) operator is presented as a cyan (red) edge. Stabilizer generators A_c and B_v^μ are defined at unit cubes (c) and vertices (v), respectively. The ground states satisfy $A_c = 1$ and $B_v^\mu = 1$ for all c, v and $\mu \in \{x, y, z\}$. Cyan strings (\mathcal{S}) and gray membranes (\mathcal{M}) represent string and membrane operators of the form $X_{\mathcal{S}} := \prod_{\ell \in \mathcal{S}} X_\ell$ and $Z_{\mathcal{M}} := \prod_{\ell \in \mathcal{M}} Z_\ell$, respectively. Fracton excitations $A_c = -1$ are created by membrane operators at their corners and colored as cyan cubes. String operators create lineon excitations at their turns and ends. The red ellipsoids represent lineons with $B_v^\mu = 1$, $B_v^{\nu \neq \mu} = -1$, where μ is indicated by the elongated directions. The extended strings and membranes $\mathcal{S}_1, \mathcal{S}_2, \mathcal{M}_1$, and \mathcal{M}_2 represent two pairs of logical operators creating no excitations due to PBC.

On a lattice of size L^3 with PBC, the X-cube model has 2^{6L-3} degenerated ground states, scaling subextensively with system size [16,20]. These ground states are indistinguishable by local operations, hence provide a fault-tolerant code Hilbert space. We can view them as $6L - 3$ logical qubits by introducing $6L - 3$ pairs of nonlocal operators ($X_{\mathcal{S}_j}, Z_{\mathcal{M}_j}$). Here, $X_{\mathcal{S}_j} := \prod_{\ell \in \mathcal{S}_j} X_\ell$ and $Z_{\mathcal{M}_j} := \prod_{\ell \in \mathcal{M}_j} Z_\ell$ are defined on *extended* strings and membranes winding around the lattice (see Fig. 1).

Error correction.—Fractons and lineons can be used to diagnose errors in the stabilizer code. For example, as illustrated in Fig. 1, a phase-flip Z error on a single qubit ℓ will cause four fractons at each of its adjacent cubes. Similarly, a single bit-flip X error will create two lineons at the vertices sharing the edge. Therefore, an ensemble of fractons or lineons can act as an A or B syndrome reflecting Z or X errors in the system.

For simplicity, we consider a situation where each qubit is affected by phase-flip and bit-flip errors independently and assume perfect measurements for all stabilizer generators. Moreover, since the X-cube model is a Calderbank-Shor-Steane (CSS) code [54], i.e., the type- A and type- B

stabilizer generators involve either purely X or Z operators, we can correct the bit-flip and phase errors separately.

The error-correction process can be described by introducing a (co)chain complex,

$$\mathbb{Z}_2^A \xrightarrow{\partial_A} \mathbb{Z}_2^Q \xrightarrow{\partial_B} \mathbb{Z}_2^B, \quad (3)$$

where \mathbb{Z}_2^A , \mathbb{Z}_2^Q , and \mathbb{Z}_2^B denote the $\mathbb{Z}_2 = \{0, 1\}$ vector spaces for labeling configurations of type- A stabilizer generators (\mathcal{A}), physical qubits (\mathcal{Q}), and type- B stabilizer generators (\mathcal{B}), respectively. The boundary maps ∂_A and ∂_B are linear and specify the qubits involved in every type- A and type- B stabilizer generator. Correspondingly, the transpose operator ∂_A^\dagger (∂_B^\dagger) maps an error configuration $\eta \in \mathbb{Z}_2^{A(B)}$ to an ensemble of fractons (lineons) created by $Z_\eta := \prod_{\ell \in \eta} Z_\ell$ ($X_\eta := \prod_{\ell \in \eta} X_\ell$). In general, $\partial_A^\dagger \circ \partial_B = \partial_B^\dagger \circ \partial_A = 0$ for all CSS codes.

Only certain error configurations are compatible with a given syndrome. Among those, error configurations are equivalent if and only if they can be connected by type- A and type- B stabilizer generators. Namely, provided $\eta - \eta' \in \text{im} \partial_A$ or $\text{im} \partial_B$, two errors η and η' will have the same effect on the encoded quantum state, where $\text{im} \partial$ denotes the image of the boundary map. Thus, the spaces of X_η and Z_η can be divided into equivalence classes by the quotients $\mathbb{Z}_2^Q / \text{im} \partial_A$ and $\mathbb{Z}_2^Q / \text{im} \partial_B$. We denote the equivalence classes as $[\eta]_X := \eta + \text{im} \partial_A$ and $[\eta]_Z := \eta + \text{im} \partial_B$, respectively.

For a possible B or A syndrome σ with probability $\text{Pr}(\sigma)$, the total probability of those equivalence classes compatible with σ satisfies $\sum_\lambda \text{pr}([\eta_\sigma + \lambda]) = \text{Pr}(\sigma)$, with $\lambda \in \mathbb{Z}_2^Q$ labeling inequivalent logical operators. The correction can be realized successfully if, for typical syndromes, there exists a *most probable* equivalence class $[\eta_\sigma^*]$ such that $\text{pr}([\eta_\sigma^*]) \rightarrow \text{Pr}(\sigma)$ in the large system limit [6]. However, this is only possible when the rate p for local X and Z errors lie below some optimal threshold values p_c^X and p_c^Z . For $p > p_c$, the error class cannot be unambiguously identified, and the code becomes ineffective. Finding the optimal error thresholds is therefore crucial to any quantum code.

Mapping to statistical-mechanical models.—An elegant and numerically preferable way to determine p_c^X and p_c^Z of the X-cube code is utilizing a statistical mapping method [6] which maps bit- and phase-flip errors to suitably chosen statistical-mechanical models.

Suppose both X and Z errors occur independently at each qubit at rate p . Then the probability the system is affected by an X or Z error configuration $\eta \in \mathbb{Z}_2^Q$ is

$$\text{pr}(\eta; p) = \prod_{\ell \in \mathcal{Q}} p^{\eta(\ell)} (1-p)^{1-\eta(\ell)} \propto \left(\frac{p}{1-p} \right)^{\sum_\ell \eta(\ell)}, \quad (4)$$

where $\eta(\ell) = 1$ or 0 on edges with or without an error.

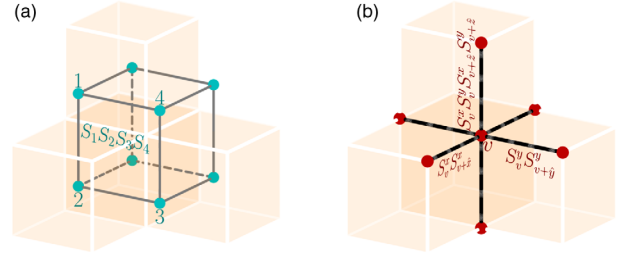


FIG. 2. Illustration of the 3D random plaquette Ising (RPI) model and the 3D random anisotropically coupled Ashkin-Teller (RACAT) model. (a) The four interacting S_c spins in the RPI model correspond to the four type- A stabilizer generators sharing an edge in the original X-cube model. (b) The RACAT model has two spins S_v^x and S_v^y at each vertex, corresponding to the two independent type- B stabilizer generators. The coupling coefficients take random signs depending on the absence and presence of local errors.

This probability can be interpreted as a Boltzmann weight by introducing an effective temperature T satisfying

$$e^{-\frac{\eta}{T}} = \frac{p}{1-p}. \quad (5)$$

Equation (5) defines the so-called *Nishimori line* and allows us to control the rate of random qubit errors through the auxiliary temperature (see Supplemental Material [43]).

Accordingly, the total probability of a bit-flip error equivalence class $[\eta]_X := \eta + \text{im} \partial_A$ is mapped to the partition function of an interacting spin Hamiltonian H_η^A ,

$$\begin{aligned} \text{pr}([\eta]_X; p) &\propto \sum_{f \in \mathbb{Z}_2^A} e^{\beta \sum_{\ell \in \mathcal{Q}} (-1)^{\eta(\ell) + \partial_A f(\ell)}} \\ &= \sum_{\{S_c = \pm 1\}} e^{-\beta H_\eta^A(\{S_c\})} =: \mathcal{Z}_\eta^A(\beta), \end{aligned} \quad (6)$$

where $\beta = 1/T$ is the inverse temperature, $f \equiv \{f(c)\}_{c \in \mathcal{A}} \in \mathbb{Z}_2^A$ represents a configuration of type- A stabilizer generators, $\partial_A f(\ell) = \sum_{c \in \partial_A^\dagger \ell} f(c)$ labels the edges of f , and $S_c = (-1)^{f(c)} \in \{\pm 1\}$ denotes effective Ising variables on the center of cubes.

The form of H_η^A realizes a 3D *random plaquette Ising* (RPI) model on a dual lattice with quenched disorder,

$$H_\eta^A(\{S_c\}) = - \sum_{\ell \in \mathcal{Q}} (-1)^{\eta(\ell)} \prod_{c \in \partial_A^\dagger \ell} S_c, \quad (7)$$

where $c \in \partial_A^\dagger \ell$ specifies the four A -stabilizer generators sharing an edge ℓ (see Fig. 2), while the probabilities of their coupling to be antiferromagnetic and ferromagnetic are p and $1-p$, respectively. Moreover, aside from a global Z_2 symmetry, H_η^A is invariant under a subsystem

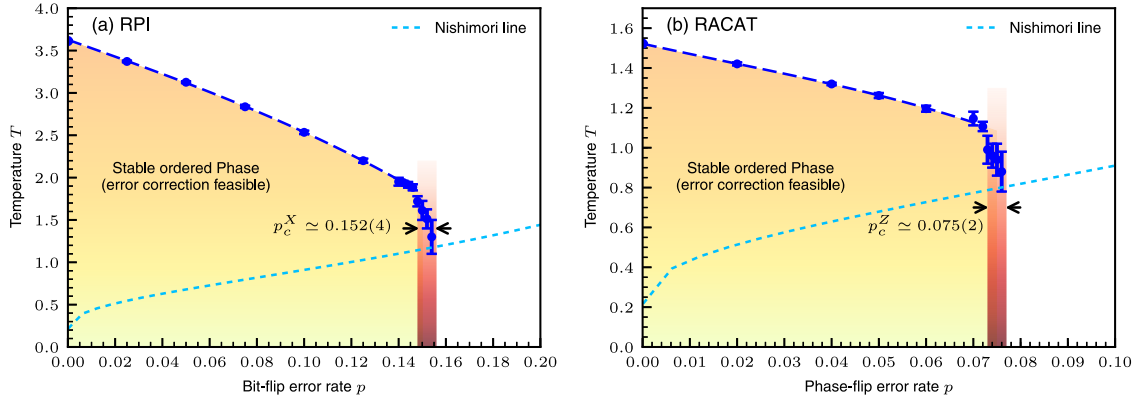


FIG. 3. Phase diagrams of the 3D RPI model and 3D RACAT model. The phase transitions are discontinuous in the low error rate (p) regions (dashed lines) but are softened to be continuous ones when approaching the threshold values $p_c^X \simeq 0.152(4)$ and $p_c^Z \simeq 0.075(2)$. The error thresholds are determined by the largest p values exhibiting an order-disorder phase transition (see Supplemental Material [43]). The effective temperature T is an auxiliary quantity and related to p by the Nishimori line (dotted line). A correctable X-cube code corresponds to the part of the Nishimori line inside the ordered phases.

symmetry flipping spins in individual planes and may be viewed as a novel random spin model.

Analogously, the modeling of a phase-flip error equivalence class $[\eta]_Z := \eta + \text{im}\partial_B$ leads to a 3D *random anisotropically coupled Ashkin-Teller* (RACAT) model with quenched disorder on the original cubic lattice,

$$H_\eta^B(\{S_v^\mu\}) = -\sum_v \sum_{\mu=x,y,z} (-1)^{\eta(\hat{e}_v^\mu)} S_v^\mu S_{v+\hat{\mu}}^\mu, \quad (8)$$

where $S_v^x = (-1)^{f_v^x}$, $S_v^y = (-1)^{f_v^y}$, and $S_v^z = S_v^x S_v^y$ are effective Ising variables, and $f \equiv \{f_v^x, f_v^y\}_v \in \mathbb{Z}_2^2$ denotes the indicator vectors for type- B stabilizer generators. The spins are coupled only along with the unit $\hat{\mu}$ direction (Fig. 2). In contrast to the usual 3D Ashkin-Teller model [55], the RACAT model Eq. (8) has the planar symmetries of flipping all S^μ and S^ν spins in an arbitrary $\mu - \nu$ plane besides a global $Z_2 \times Z_2$ symmetry.

The disorder-free limits ($p = 0$) of H_η^A and H_η^B are dual to each other [56], as for general fracton and topological CSS codes [43]. There is no exact duality in the presence of disorder, nevertheless, our results suggest an approximate duality relation between the error thresholds p_c^X and p_c^Z [43].

On the side of the statistical-mechanical models, the relative probability between two X (or Z) error equivalence classes under the error rate p is given by the difference between their free energies,

$$\frac{\text{pr}([\eta + \lambda]_{X(Z)}; p)}{\text{pr}([\eta]_{X(Z)}; p)} = \frac{\mathcal{Z}_{\eta+\lambda}^{A(B)}(\beta)}{\mathcal{Z}_\eta^{A(B)}(\beta)} = e^{-\beta \delta \mathcal{F}_{\eta,\lambda}^{A(B)}}, \quad (9)$$

where $\lambda \in \mathbb{Z}_2^Q$ represents logical X (or Z) operators of the X-cube model and can flip a sequence of coupling coefficients in H_η^A (H_η^B). The condition of existing

$\text{pr}([\eta_\sigma^*]_{X(Z)}) \rightarrow \text{Pr}(\sigma)$ for the *most probable* equivalence class $[\eta_\sigma^*]_{X(Z)}$ requires that the free energy to introduce a nontrivial string (membrane) defect ($\lambda \neq 0$) diverges in the thermodynamical limit, namely, $\delta \mathcal{F}_{\eta,\lambda}^{A(B)} \rightarrow \infty$ (see Supplemental Material [43]). This is only possible when H_η^A and H_η^B are in their ordered phases. Hence p_c^X and p_c^Z can be determined from the order-disorder phase transitions of the two random spin models.

Error thresholds and phase diagrams.—The phase diagrams of the RPI and RACAT models are shown in Fig. 3 obtained by large-scale parallel tempering Monte Carlo simulations. We locate the phase transitions by cross-checking the energy histogram, specific heat, order parameter, its susceptibility, and the correlation length [43].

To construct the appropriate order parameters, the planar symmetries of H_η^A and H_η^B have to be taken into account as they can lead to trivial cancellation of local orders. For the RPI model, we define

$$Q^A := \frac{1}{L^3} \sum_{z=0}^{L-1} \left[\left\langle \left| \sum_{x,y=0}^{L-1} S_{c(x,y,z)} S_{c(x,y,z+1)} \right| \right\rangle \right], \quad (10)$$

with $\langle \cdot \rangle$ and $[\cdot]$ denoting the thermal and disorder average, respectively. The inner sum in Eq. (10) involves a sub-extensive number ($\propto L^2$) of spins, while the norm enforces the planar-flip invariance [57]. Thus, Q^A defines a long-range order which is *subdimensional* and made of *planelike* objects.

The order parameter for the RACAT model is constructed similarly;

$$Q^B := \frac{1}{L^3} \sum_{x,y=0}^{L-1} \left[\left\langle \left| \sum_{z=0}^{L-1} S_{v(x,y,z)}^z \right| \right\rangle \right], \quad (11)$$

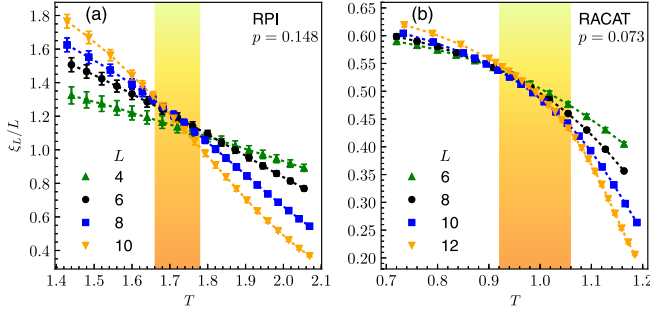


FIG. 4. Normalized second-moment correlation length ξ_L/L for the 3D RPI (a) and RACAT (b) model close to the error thresholds $p_c^X \simeq 0.152(4)$ and $p_c^Z \simeq 0.075(2)$. For a second-order phase transition the curves for different system sizes intersect near the critical temperature T_c . The shaded areas show a conservative estimate of T_c . Such intersections cannot be recognized for $p > p_c^X$ or p_c^Z where we conclude no phase transition.

which describes an order for extended *line* objects. Here, the S_v^z spins are taken for simplicity, as the three Ising variables in Eq. (8) are permutable.

At low X and Z error rates, the energy histograms reveal a first-order phase transition for both H_η^A and H_η^B [43]. This agrees with previous studies on the disorder-free ($p = 0$) limit of the two models [56,57]. Hence the transition temperatures can be estimated in a relatively straightforward way [43].

For larger p , the phase transitions are softened to continuous ones in line with the Imry-Ma scenario [58,59]. We can then locate the transitions by studying the second-moment correlation length

$$\xi_L := \frac{1}{2 \sin(|\mathbf{k}_{\min}|/2)} \left(\frac{\tilde{G}(\mathbf{0})}{\tilde{G}(\mathbf{k}_{\min})} - 1 \right)^{1/2}, \quad (12)$$

where $\tilde{G}(\mathbf{k}) := \sum_{\mathbf{r}} G(\mathbf{r}) e^{-i\mathbf{k}\cdot\mathbf{r}}$ is a Fourier transform of the spatial correlator $G(\mathbf{r})$, and \mathbf{k}_{\min} denotes any smallest nonzero wave vector [60].

The spatial correlators related to the order parameters Q^A and Q^B are given by

$$G^A(\mathbf{r}) := \frac{1}{L^3} \sum_{c \in \mathcal{L}} [\langle S_c S_{c+\hat{z}} S_{c+(\mathbf{r},0)} S_{c+(\mathbf{r},\hat{z})} \rangle], \quad (13)$$

$$G^B(r) := \frac{1}{L^3} \sum_{v \in \mathcal{L}} [\langle S_v^z S_{v+r\hat{z}}^z \rangle], \quad (14)$$

so that $G^{A(B)}(\mathbf{r}) \rightarrow [Q^{A(B)}]^2$ in the limit of $|\mathbf{r}| \rightarrow \infty$.

Provided a continuous phase transition exists, ξ_L/L is expected to be scaled as $g(L^{1/\nu}(T - T_c))$ near the critical point, and the curves for different system sizes should intersect at $(T_c, g(0))$, where g is a universal scaling function and ν denotes the critical exponent of ξ .

We can use this property to search the largest error rates where H_η^A and H_η^B continue showing a continuous phase transition, which in turn implies the error thresholds of the X-cube code.

Our simulations show that the $\xi_L(T)/L$ curves exhibit clear intersections up to an error rate $p_c^X \simeq 0.152(4)$ for the RPI model and $p_c^Z \simeq 0.075(2)$ for the RACAT model (see Fig. 4 and also Supplemental Material [43]). Thereafter, a clear intersection cannot be recognized [43], indicating lack of an order-disorder transition. Namely, for error rates larger than p_c^X and p_c^Z , H_η^A and H_η^B host no long-range order, and the X-cube code hence becomes uncorrectable.

Conclusions.—The X-cube model is the archetypal stabilizer code exhibiting the fascinating quantum physics of fracton topological orders. In this Letter we investigated its capability as a quantum memory through a combination of theoretical analyses and detailed numerical simulations. We estimated its optimal error thresholds as $p_c^X \simeq 15.2(4)\%$ against bit-flip noise and $p_c^Z \simeq 7.5(2)\%$ against phase-flip noise, featuring a remarkably higher minimum error rate (7.5%) compared to the 3D toric code (3.3%) [41,42] and color code (1.9%) [38]. Our Letter establishes the general connection between the fault tolerance of fracton codes and statistical-mechanical models with subsystem symmetries. The Pauli error thresholds in any CSS code with zero-encoding rate [6,33,34,38] obey the inequality $H(p_c^X) + H(p_c^Z) \leq 1$ imposed by the quantum Gilbert-Varshamov bound [61–63], where $H(p) := -p \log_2(p) - (1-p) \log_2(1-p)$ is the Shannon entropy. Our results give $H(p_c^X) + H(p_c^Z) \simeq 1.00(2)$, which not only satisfies this constraint but is close to its upper bound, similar to the situations found in conventional topological codes [33,38,64]. We formulate this near saturation via an approximate duality in the Supplemental Material [43] and conjecture it for general fracton and topological CSS codes. Our Letter can guide further studies of fracton models, and the approximate duality predicts even higher thresholds for the self-dual checkerboard [16] and Haah’s [13] codes.

The data used in this work will be made available in Ref. [65].

H. S. and M. A. M.-D. acknowledge support from the Spanish MINECO grants MINECO/FEDER Projects FIS2017-91460-EXP, PGC2018-099169-B-I00 FIS-2018, and with O. V. from CAM/FEDER Project No. S2018/TCS-4342 (QUITEMAD-CM). H. S. has also been supported by the Natural Sciences and Engineering Research Council of Canada and by the National Natural Science Foundation of China (Grant No. 12047503). M. A. M.-D. has also been supported by MCIN with funding from European Union Next-GenerationEU (PRTR-C17.I1) and the Ministry of Economic Affairs Quantum ENIA project, and partially by the U.S. Army Research Office through

Grant No. W911NF-14-1-0103. J. S.-K., K. L., and L. P. acknowledge support from FP7/ERC Consolidator Grant QSIMCORR, No. 771891, and the Deutsche Forschungsgemeinschaft (DFG, German Research Foundation) under Germany's Excellence Strategy—EXC-2111–390814868. The project and research is part of the Munich Quantum Valley, which is supported by the Bavarian state government with funds from the High-tech Agenda Bayern Plus. Our simulations make use of the ALPSCore library [66] and the TKSVMLibrary [67,68].

*ke.liu@lmu.de

†mardel@fis.ucm.es

- [1] J. Preskill, Fault-tolerant quantum computation, in *Introduction to Quantum Computation and Information* (World Scientific, Singapore, 1998), pp. 213–269, 10.1142/9789812385253_0008.
- [2] M. A. Nielsen and I. L. Chuang, *Quantum Computation and Quantum Information* (Cambridge University Press, Cambridge, England, 2000).
- [3] A. Galindo and M. A. Martín-Delgado, *Rev. Mod. Phys.* **74**, 347 (2002).
- [4] A. Kitaev, *Ann. Phys. (Amsterdam)* **303**, 2 (2003).
- [5] H. Bombin and M. A. Martin-Delgado, *Phys. Rev. Lett.* **97**, 180501 (2006).
- [6] E. Dennis, A. Kitaev, A. Landahl, and J. Preskill, *J. Math. Phys. (N.Y.)* **43**, 4452 (2002).
- [7] H. Bombin and M. A. Martin-Delgado, *Phys. Rev. Lett.* **98**, 160502 (2007).
- [8] S. B. Bravyi and A. Y. Kitaev, arXiv:quant-ph/9811052.
- [9] S. Bravyi and R. König, *Phys. Rev. Lett.* **110**, 170503 (2013).
- [10] S. Aaronson and D. Gottesman, *Phys. Rev. A* **70**, 052328 (2004).
- [11] C. Chamon, *Phys. Rev. Lett.* **94**, 040402 (2005).
- [12] S. Bravyi, B. Leemhuis, and B. M. Terhal, *Ann. Phys. (Amsterdam)* **326**, 839 (2011).
- [13] J. Haah, *Phys. Rev. A* **83**, 042330 (2011).
- [14] B. Yoshida, *Phys. Rev. B* **88**, 125122 (2013).
- [15] S. Vijay, J. Haah, and L. Fu, *Phys. Rev. B* **92**, 235136 (2015).
- [16] S. Vijay, J. Haah, and L. Fu, *Phys. Rev. B* **94**, 235157 (2016).
- [17] H. Ma, E. Lake, X. Chen, and M. Hermele, *Phys. Rev. B* **95**, 245126 (2017).
- [18] S. Vijay and L. Fu, arXiv:1706.07070.
- [19] R. M. Nandkishore and M. Hermele, *Annu. Rev. Condens. Matter Phys.* **10**, 295 (2019).
- [20] H. Song, A. Prem, S.-J. Huang, and M. A. Martin-Delgado, *Phys. Rev. B* **99**, 155118 (2019).
- [21] A. Prem, S.-J. Huang, H. Song, and M. Hermele, *Phys. Rev. X* **9**, 021010 (2019).
- [22] X.-G. Wen, *Phys. Rev. Res.* **2**, 033300 (2020).
- [23] J. Wang, *Phys. Rev. Res.* **4**, 023258 (2022).
- [24] D. Aasen, D. Bulmash, A. Prem, K. Slagle, and D. J. Williamson, *Phys. Rev. Res.* **2**, 043165 (2020).
- [25] T. Devakul, S. A. Parameswaran, and S. L. Sondhi, *Phys. Rev. B* **97**, 041110(R) (2018).
- [26] M. Mühlhauser, M. R. Walther, D. A. Reiss, and K. P. Schmidt, *Phys. Rev. B* **101**, 054426 (2020).
- [27] C. Zhou, M.-Y. Li, Z. Yan, P. Ye, and Z. Y. Meng, *Phys. Rev. Res.* **4**, 033111 (2022).
- [28] S. Bravyi and J. Haah, *Phys. Rev. Lett.* **111**, 200501 (2013).
- [29] B. J. Brown and D. J. Williamson, *Phys. Rev. Res.* **2**, 013303 (2020).
- [30] R. Verresen, N. Tantivasadakarn, and A. Vishwanath, arXiv:2112.03061.
- [31] N. E. Myerson-Jain, S. Yan, D. Weld, and C. Xu, *Phys. Rev. Lett.* **128**, 017601 (2022).
- [32] Y. You and F. von Oppen, *Phys. Rev. Res.* **1**, 013011 (2019).
- [33] H. G. Katzgraber, H. Bombin, and M. A. Martin-Delgado, *Phys. Rev. Lett.* **103**, 090501 (2009).
- [34] H. Bombin, R. S. Andrist, M. Ohzeki, H. G. Katzgraber, and M. A. Martin-Delgado, *Phys. Rev. X* **2**, 021004 (2012).
- [35] H. G. Katzgraber, H. Bombin, R. S. Andrist, and M. A. Martin-Delgado, *Phys. Rev. A* **81**, 012319 (2010).
- [36] R. S. Andrist, H. G. Katzgraber, H. Bombin, and M. A. Martin-Delgado, *New J. Phys.* **13**, 083006 (2011).
- [37] R. S. Andrist, H. G. Katzgraber, H. Bombin, and M. A. Martin-Delgado, *Phys. Rev. A* **94**, 012318 (2016).
- [38] A. Kubica, M. E. Beverland, F. Brandão, J. Preskill, and K. M. Svore, *Phys. Rev. Lett.* **120**, 180501 (2018).
- [39] O. Viyuela, S. Vijay, and L. Fu, *Phys. Rev. B* **99**, 205114 (2019).
- [40] D. Vodola, M. Rispler, S. Kim, and M. Müller, *Quantum* **6**, 618 (2022).
- [41] C. Wang, J. Harrington, and J. Preskill, *Ann. Phys. (Amsterdam)* **303**, 31 (2003).
- [42] T. Ohno, G. Arakawa, I. Ichinose, and T. Matsui, *Nucl. Phys. B* **697**, 462 (2004).
- [43] See Supplemental Material at <http://link.aps.org/supplemental/10.1103/PhysRevLett.129.230502> for the Kramers-Wannier duality of CSS code, more details of the error correction process, the proof for the absence of glass order along the Nishimori line, and details of numerical simulations, which contains additional Refs. [44–53].
- [44] F. Y. Wu and Y. K. Wang, *J. Math. Phys. (N.Y.)* **17**, 439 (1976).
- [45] H. Nishimori, *Statistical Physics of Spin Glasses and Information Processing: An Introduction* (Oxford University Press, Oxford, New York, 2001).
- [46] J. Lee and J. M. Kosterlitz, *Phys. Rev. Lett.* **65**, 137 (1990).
- [47] J. Lee and J. M. Kosterlitz, *Phys. Rev. B* **43**, 3265 (1991).
- [48] S. Jin, A. Sen, and A. W. Sandvik, *Phys. Rev. Lett.* **108**, 045702 (2012).
- [49] R. J. Baxter, *J. Phys. C* **6**, L445 (1973).
- [50] M. Mueller, W. Janke, and D. A. Johnston, *Phys. Rev. Lett.* **112**, 200601 (2014).
- [51] M. S. S. Challa, D. P. Landau, and K. Binder, *Phys. Rev. B* **34**, 1841 (1986).
- [52] H. G. Katzgraber, S. Trebst, D. A. Huse, and M. Troyer, *J. Stat. Mech.* (2006) P03018.
- [53] B. Efron and R. J. Tibshirani, *An Introduction to the Bootstrap* (CRC Press, New York, 1994), 10.1201/9780429246593.
- [54] A. R. Calderbank, E. M. Rains, P. W. Shor, and N. J. A. Sloane, *Phys. Rev. Lett.* **78**, 405 (1997).

- [55] R. V. Ditzian, J. R. Banavar, G. S. Grest, and L. P. Kadanoff, *Phys. Rev. B* **22**, 2542 (1980).
- [56] D. A. Johnston and R. P. K. C. M. Ranasinghe, *J. Phys. A* **44**, 295004 (2011).
- [57] D. A. Johnston, M. Mueller, and W. Janke, *Eur. Phys. J. Special Topics* **226**, 749 (2017).
- [58] Y. Imry and S.-k. Ma, *Phys. Rev. Lett.* **35**, 1399 (1975).
- [59] Y. Imry and M. Wortis, *Phys. Rev. B* **19**, 3580 (1979).
- [60] W. Janke, Monte Carlo methods in classical statistical physics, in *Computational Many-Particle Physics*, edited by H. Fehske, R. Schneider, and A. Weiße (Springer Berlin Heidelberg, Berlin, Heidelberg, 2008), pp. 79–140.
- [61] E. N. Gilbert, *Bell Syst. Tech. J.* **31**, 504 (1952).
- [62] R. R. Varshamov, *Doklady Akad. Nauk, S.S.S.R.* **117**, 739 (1957), <http://mi.mathnet.ru/dan22571>.
- [63] A. R. Calderbank and P. W. Shor, *Phys. Rev. A* **54**, 1098 (1996).
- [64] H. Nishimori, *J. Stat. Phys.* **126**, 977 (2007), where a different convention is used with $1 - p$ (instead of p) denoting the probability for antiferromagnetic coupling, and see also the references therein.
- [65] https://github.com/KeLiu-04/Xcube_data.
- [66] A. Gaenko, A. Antipov, G. Carcassi, T. Chen, X. Chen, Q. Dong, L. Gamper, J. Gukelberger, R. Igarashi, S. Iskakov, M. Könz, J. LeBlanc, R. Levy, P. Ma, J. Paki, H. Shinaoka, S. Todo, M. Troyer, and E. Gull, *Comput. Phys. Commun.* **213**, 235 (2017).
- [67] J. Greitemann, K. Liu, and L. Pollet, *Phys. Rev. B* **99**, 060404(R) (2019).
- [68] K. Liu, J. Greitemann, and L. Pollet, *Phys. Rev. B* **99**, 104410 (2019).